ACS APPLIED MATERIALS & INTERFACES

Research Article

www.acsami.org

Large Area Nanostructured Arrays: Optical Properties of Metallic Nanotubes

Katja Fröhlich,[†,‡] Pejman Hojati-Talemi,[†] Matthew Bishop,[†,§] Kamil Zuber,[†] Peter Murphy,[†] and Drew Evans*[,†]

[†]ETH, Zurich, Wolfgang-Pauli-Str. 10, 8093 Zurich, Switzerland

[‡]Mawson Institute, University of South Australia, Adelaide, 5095, Australia

[§]Department of Chemistry, University of Bath, Bath, BA2 7AY, U.K.

Supporting Information

ABSTRACT: In this study, large area metallic nanotube arrays on flexible plastic substrates are produced by templating the growth of a cosputtered alloy using anodized aluminum oxide membranes. These nanotube arrays are prepared over large areas (ca. squared centimeters) by reducing the residual stress within the thin multilayered structure. The nanotubes are approximately 20 nm in inner diameter, having walls of <10 nm in thickness, and are arranged in a close packed configuration. Optically the nanotube arrays exhibit light trapping behavior (not plasmonic), where the reflectivity is less than 15% across the visible spectra compared to >40% for a flat sample using the same alloy. When the nanotubes are exposed to high relative humidity, they spontaneously fill, with a concomitant change in their visual appearance. The filling of the nanotubes is confirmed using contact angle measurements, with the nanotubes displaying a strong hydrophilic character compared to the weak behavior of the flat sample. The ability to easily fabricate large area nanotube arrays which display exotic behavior paves the way for their uptake in real world applications such as sensors and solar energy devices.

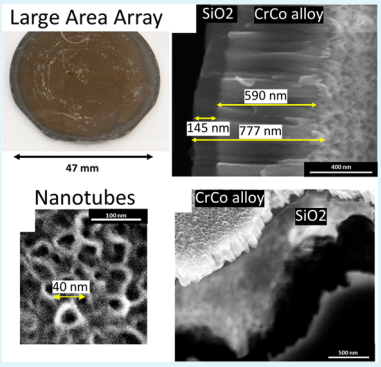

KEYWORDS: *hydrophilic effect, nanotechnology, nanotubes, optics, template synthesis*

INTRODUCTION

Functional nanostructured arrays display exotic optical, electrical, biological, and wetting behavior when compared to the unstructured or flat surfaces of the same material. Such interesting properties are also observed in naturally occurring nanostructures such as those on a moth eye,[1,2] Lotus leaf,[3] and butterfly wing[4] with the biomimicking of such structures attracting much interest among scientists working in areas such as fuel cells,[5] sensors,[6,7] solar cells,[8,9] microfluidic systems, and micro-optical components.[10] This is why a wide range of methods and materials are reported for preparation of such nanostructured surfaces. Metals or metallic alloys due to their interesting physical properties are of special interest.[11,12] Methods such as electrodeposition,[5] electroplating,[13] nanomolding amorphous metal,[14] vapor and wet chemical based deposition,[15] thermal vacuum deposition,[16] and electron beam techniques[10] are examples of techniques used for depositing metals onto nanotemplates such as anodic aluminum oxide (AAO). The well-explored chemistry of AAO, and its well-defined geometry,[1,17] has made it one the most common and inexpensive nanotemplates available.

But despite all these advantages, there have been limited reports of the large area nanostructured arrays (areas greater than a few squared micrometers) that are required for real world applications. One of the main drawbacks of these technologies is the lack of mechanical stability of these types of nanostructures. This includes poor mechanical properties of individual tubes, residual stress within the structures, and high intertube/rod interaction (e.g., van der Waals forces) that may result in the formation of aggregates,[18] cracking of the samples to create isolated domains, and stress induced curling of arrays. Due to these problems most of the previous literature has only reported small area samples (ca squared micrometers),[16] ultimately limiting the practical applications of these arrays. Added issues arise from the procedure employed to remove the template from the nanostructured array, again providing restrictions to obtaining larger area samples (ca squared centimeters). This provides the motivation for achieving and reporting a technique to obtain large area samples (ca squared centimeters) which can then lead to applications in real world devices and products. The other shortcoming of current techniques is the restriction of each technique to a limited number of metals or alloys (due to their chemical, electrochemical, and mechanical properties). Thus, developing a fabrication technique that can overcome these problems would be a major step toward implementation of nanostructured metallic arrays in real world applications. Among the proposed techniques, magnetron sputtering can be used to deposit a wide

Received: February 22, 2013
Accepted: April 12, 2013
Published: April 12, 2013

   dx.doi.org/10.1021/am400671n | ACS Appl. Mater. Interfaces 2013, 5, 3937−3942

range of materials, from metals to metal alloys and oxides, with the ability to control properties of the deposited film such as grain size and residual stress. Properties such as these are important when fabricating nanostructures over large areas.

In this paper, we present an approach to prepare large scale nanostructured thin films by cosputtering[19] of metals and metal oxides, while controlling stresses within the films. Beside capability of fabricating large scale homogeneous nanostructured arrays, the main advantage of this technique is that it can be used for making nanostructures of a wide range of metals, metal oxides, alloys, and composites with precise control on the composition ratio. The method presented herein is exemplified by the previously studied nanocomposite alloys deposited by cosputtering,[19−21] specifically $CrCo_{0.04}$. Using this cosputtering technique, we prepared nanostructured surfaces consisting of vertically aligned nanotubes with an internal diameter of 20 nm, with the optical properties and physical morphology of these arrays then characterized.

EXPERIMENTAL SECTION

The samples investigated were fabricated by sequentially cosputtering Cr and Co metal in an Ar environment[19] onto AAO membranes (Anopore Membrane Disc, 0.02 μm pore diameter, 47 mm total diameter, Whatman GmbH Dassel Germany). Cr and Co were sputtered at 1 kW and 28 W respectively from high purity 5 in. × 12 in. rectangular and 3 in. diameter circular target, respectively, where the thickness of the alloy film was controlled by changing the deposition time of the sputtering process. The internal stress of the alloy film was tuned by changing the sputtering conditions, namely the Argon (Ar) flow rate. An Ar gas flow of 60 standard cubic centimeters per minute (sccm) during deposition of the $CrCo_{0.04}$ film allowed for tensile films to be formed[22] to reduce the occurrence of delamination and thus improving the mechanical stability. X-ray photoelectron spectroscopy (XPS, Specs) was used to determine the atomic composition for the $CrCo_x$ alloy.

To further modify the residual stress of the multilayer coating and cap the remaining AAO membrane pores, an additional layer of SiO_2 was sputtered onto the $CrCo_{0.04}$ film (Figure 1B). When Si was sputtered at a power of 2.2 kW (in an Ar + O_2 gas atmosphere), the residual stress of the multilayer coating was reduced with a concomitant increase in mechanical stability. By comparison, a sample sputtered under different condition (25 sccm Ar gas flow during $CrCo_{0.04}$ sputtering and 2.4 kW applied power during SiO_2 sputtering), reduced the mechanical stability of the multilayer coating due to a relatively higher residual film stress. To further improve the mechanical stability for this specific sample, it was annealed for 1 h at 640 °C to decrease the residual film stress.

After preparing the sputtered films on the AAO membrane, the AAO membrane must be removed in order to expose the nanostructured coating. Before this can occur, the film must be attached to a supporting substrate because the free-standing nanostructured coatings are fragile and disintegrate immediately. To attach the nanostructured coatings to a substrate, either UV curable glue (4052-4, Epotek) or Epoxy glue (5 min epoxy 5-208 20845, Devcon) were spin-coated onto a glass slide for 60 s at 2500 rpm. In the instance of the UV glue, after precuring for 6−7 s under UV light (Model 2000 Flood, Dymax), the nanostructured coating was placed face down onto the coated glass slide (Figure 1C). This gluing process was observed to induce a large residual stress in the multilayer structure.

In contrast to this preparation, the epoxy glue was coated onto a flexible transparent plastic film. The use of the epoxy glue eliminated the need for precuring before bonding together the substrate and nanostructured coating. Using the flexible plastic film instead of a glass slide had the advantage that it easily conformed to the shape of the nanostructured film membrane composite (no extra pressure had to be applied to bring substrate and film into contact). The epoxy glue was cured for at least 1 h at room temperature and a relative humidity of 35% ± 5%. Slow curing for the adhesive glue aided in maintaining a low residual stress in the multilayer coating, thus enabling the nanostructured coating to cover large areas without delaminating.

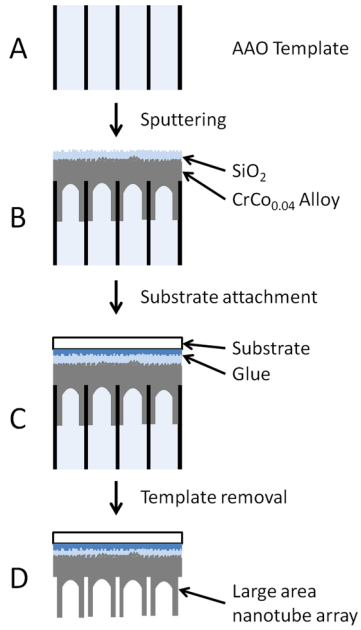

Figure 1. Scheme for the fabrication of nanotube arrays of $CrCo_{0.04}$ using an AAO membrane. (B) $CrCo_{0.04}$ alloy followed by SiO_2 is deposited via sputtering onto the AAO membrane. (C) This is then attached to a substrate (glass slide or flexible plastic film) using a curable glue (UV curable or epoxy). (D) The AAO membrane is then removed in a 10 wt % KOH solution to expose the nanostructured coating.

The samples were then immersed in a 10 wt % KOH (Analytical Reagent, min 85%, Chem-Supply) solution for 15 min. Once the membrane was fully dissolved, the nanostructured coating and substrate were gently washed with an excess of Milli Q water and dried at 70 °C on a heating plate. A schematic image of the resulting sample is shown in Figure 1D.

RESULTS AND DISCUSSION

The morphology of the $CrCo_{0.04}$ alloy coating is influenced by the sputtering time. Short sputtering times result in a nonpercolating alloy film and collapsed nanorods (Supporting Information Figure S1), compared to longer times displaying a dense film with stable nanotubes as shown in Figure 2A. The SEM image depicts the nanotube structure in a densely packed configuration. EDX measurements verify the near complete removal of the AAO membrane (Figure 2B) due to the observation of minimal amounts of Al.

Given the nanostructure of the coating is observed to be nanotubes, the sputtered atoms must be preferentially adhering to the pore walls of the AAO membranes thus creating the tubular shapes. This is in contrast to the mechanism for thermally evaporated films presented by Losic et al.[16] to explain their observation of solid nanorods template by the AAO membrane. The change in observed mechanism highlights the important role that the deposition technique plays and not the material in isolation, in defining the nanostructure.

To make the nanostructure array robust for large area samples, additional thin layers are placed between the array and the substrate. In the coating architecture presented in Figure 1, the additional SiO_2 layer not only stabilizes the film

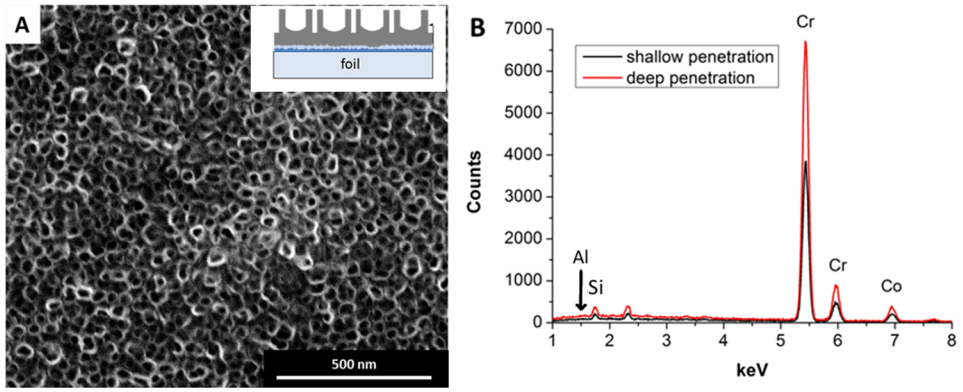

Figure 2. (A) SEM and schematic image (inset) of nanotube coating (nanotube array + epoxy glue + flexible plastic film). (B) EDX measurement confirming full removal of the AAO membrane.

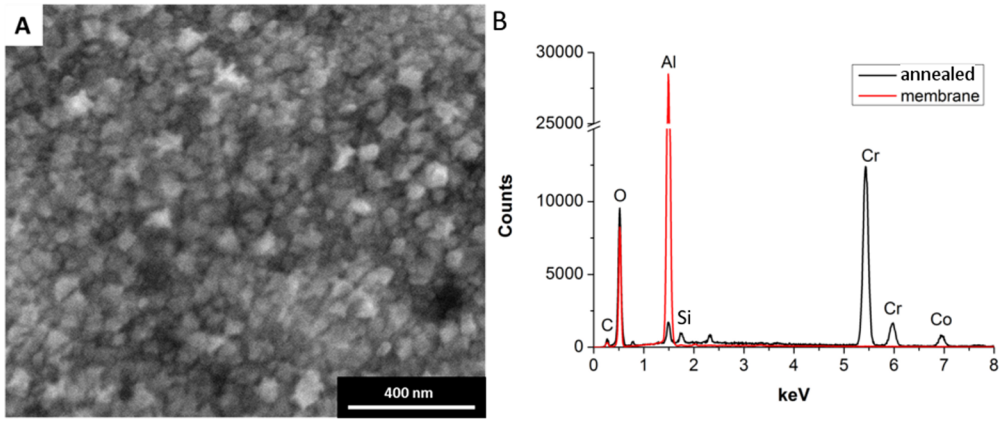

Figure 3. (A) SEM image of the nanostructured sample after annealing for 1 h at 640 °C. The coating appears as a random structure with no nanotubes. (B) EDX measurement made on the AAO membrane after detaching it from the annealed alloy film showing no residual alloy remains (atomic percent of Cr and Co < 0.05%).

mechanically, it also acts as a barrier to glue penetration through the $CrCo_{0.04}$ film and the AAO membrane. In the absence of the SiO_2 layer, glue penetrates through the nanotube array into the AAO membrane, thus protecting it from the KOH solution (effectively encapsulating the nanostructure within the AAO membrane). SEM images and EDX measurements (Supporting Information Figure S2) of the samples without the SiO_2 layer provides evidence that the AAO membrane was not completely dissolved, therefore leaving patches of membrane on the nanostructured coating (in some cases the nanotube structures were not visible at all).

Another aspect for consideration is the conditions under which the nanotube arrays are fabricated; namely their deposition and postprocessing. When the "typical" sputtering conditions[19] were employed for the $CrCo_{0.04}$ and SiO_2, the samples showed high residual stresses which often led to delamination from the substrate and curling up of the film (Supporting Information Figure S3). This effect is the primary limiting factor to engineering large area nanostructured arrays, and hence it is important to minimize the residual stress. One method to relax residual stress within a material is to subject them to a postprocessing annealing step. In this study the sputtered membranes were annealed at 640 °C for 1 h. Unfortunately, the membranes suffered extreme bending during the annealing and became very brittle. During the subsequent KOH treatment, the membrane did not dissolve, but simply detached from the nanostructured coating. According to the membrane manufacturer, the membranes are only stable up to 40 °C and SEM investigation indicated a major pore size change after the annealing (from a radius of 20 nm to greater than 50 nm, Supporting Information Figure S4). Furthermore, upon annealing the nanotubes vanished and a random rough surface replaced them (Figure 3A). EDX measurement of both the film and the detached membrane confirm that the nanostructured coating and membrane have separated despite the degraded nanostructure. The film contains a low atomic percentage of Al whereas the membrane contains no Cr or Co (Figure 3B). The randomly rough structure arises from the recrystallization of the $CrCo_{0.04}$ into the larger grain structure observed for the native unstructured material (Supporting Information Figure S5), thus destroying the nanotube structure. By employing sputtering as the method for fabrication, the limitation of the materials grain size has been overcome.

An alternate means to control the residual stress is to modify the sputtering conditions;[22] for example changes in the gas pressure, power applied to the magnetron target, and substrate temperature influence the residual stress of the deposited material. These changes in deposition parameters are responsible for changes in the film structure (grain size and growth of the film), as described by the structure zone model,[23] which then defines the films macroscopic properties (structure−property relationship). Increasing the Ar gas flow (from 25 to 60 sccm) during $CrCo_{0.04}$ deposition and reducing the power (from 2.4 to 2.2 kW) during deposition of the SiO_2

layer, led to stable large area nanostructured coatings with the retention of the nanotubes (Figure 4A). This demonstrates how the sputtering process can be used to prepare large area nanotube arrays.

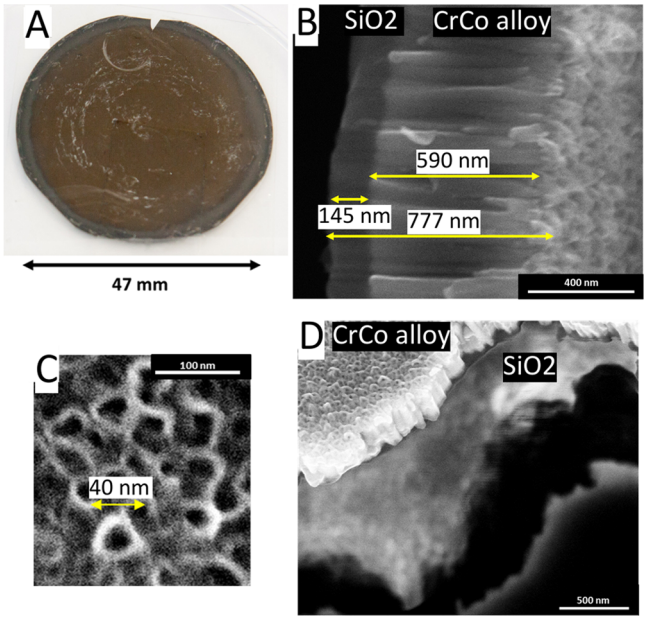

Figure 4. (A) Large area $CrCo_{0.04}$ nanotube coating on a flexible plastic foil. (B–D) SEM image of $CrCo_{0.04}$ and SiO_2 thin film. (B) Side view of the multilayer coating. (from left to right) SiO_2 layer, $CrCo_{0.04}$ layer with nanotubes. (C) Top view of sample depicting the size of individual nanotubes. (D) Sliding of the two sputtered layers (upper layer $CrCo_{0.04}$, lower layer SiO_2) during sample preparation for SEM imaging.

Looking at the film in more detail (Figure 4B) shows an approximate $CrCo_{0.04}$ and SiO_2 film thickness of 590 and 145 nm, respectively (determined from cross-sectional SEM imaging). The nanotubes themselves have a height of around 12 nm and outer diameters of 30–50 nm (Figure 4C). Although the SiO_2 film is rather thin compared to the $CrCo_{0.04}$ layer, it effectively closes the remaining pores and prevents the penetration of the glue to the surface of the sample.

The fabrication process described herein can be generalized beyond $CrCo_{0.04}$ to other materials, broadening the scope of potential applications for the nanotube arrays. For example, materials such as silicon dioxide and tungsten can be used to generate the large area nanotube arrays. These specific coating examples are presented as nanotube arrays in Supporting Information Figure S6.

The nanostructuring is expected to influence the macroscopic properties of the large area array. A very simple assessment of this influence can be made by comparing the optical properties (reflectivity) of the various nanostructured coatings to that of an untextured flat coating. As shown in Figure 5, the untextured sample has a high reflectivity over all wavelengths, which appears as a silver mirror. The annealed sample has the highest visible reflectivity in the yellow spectra region, thus it is golden in appearance. As shown by Lyvers et al.,[24] the reflectance spectra of nanorod arrays changes with varying nanorod height and dielectric medium. In their case, the plasmonic effect occurs if the nanorod lengths are in the same size range as the wavelength of light. The change of color observed herein for the annealed sample cannot be due to the plasmonic effect, as the height of the structures is much shorter than the observed wavelength maxima.

The nanotube array is low in reflectivity across all the wavelengths and lacks plasmonic behavior. Low reflectivity at 0° tilting angle is an indication of light trapping, given the unstructured flat coating is quite reflective. Compared to other studies, where low reflectivity was achieved with long nanotubes,[25] the nanotubes in this study are relatively short.

In addition to optical applications, nanostructuring is responsible for controlling the way the coating is wet with water or oil. This exotic wetting behavior is quantified from measurements of the contact angle of a water droplet impinging on the coating surface and, ultimately, allows for the mechanical stability of the nanostructure against capillary forces to be observed. Table 1 reports the advancing contact angle for the

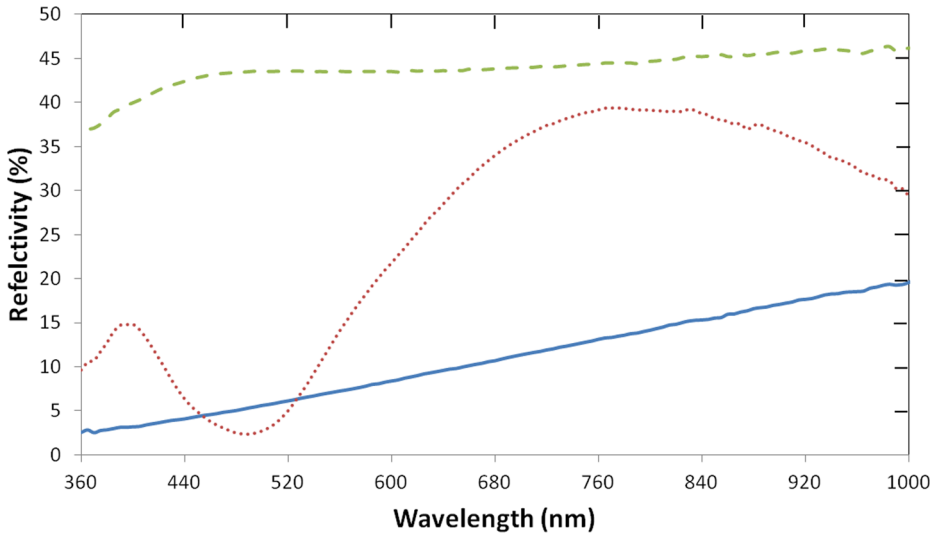

Figure 5. Reflectivity (0° angle of incident) as a function of wavelength for the various alloy coatings. The flat coating (dashed line) displays mirror-like reflectivity, while the nanostructure of the annealed coating (dotted line) and nanotube coating (solid line) display reduced reflectivity. In the case of the nanotube coating, the reflectivity of <15% across the visible spectrum indicates light tapping behavior.

Table 1. Contact Angle Measurements on the Various $CrCo_{0.04}$ Alloy Coatings

	advancing contact angle		receding contact angle	
sample	average [deg]	std [deg]	average [deg]	std [deg]
untextured	87.0	9.5	20.7	4.6
nanotubes	30.7	2.2	11.8	1.4
annealed	28.3	4.4	14.3	2.1

respective samples, with a weak hydrophilic angle approaching 90° for the flat unstructured coating, whereas the nanotube and the annealed coatings show strongly hydrophilic behavior with an angle of less than 30° (the difference in receding angles is shown in Figure 6). The high hysteresis between the advancing and the receding contact angle provide evidence of a rough surface with a high pinning effect. Roughness of a coating enhances the underlying wetting properties defined by its chemistry, thus the nanostructuring should enhance the hydrophilic character defined by the $CrCo_{0.04}$ alloy.[26] This is indeed the case, with the nanotube coating leading to improved wetting by water. Due to the contact angle of the flat unstructured coating being slightly less than 90°, the water droplets do not rest on top of the nanotubes but penetrate into the pores defined by the nanotubes.

Pores of nanometer dimensions are known to spontaneously fill with liquid due to capillary condensation.[27] The pores defined by the nanotube structure are calculated (using the Kelvin equation[28]) to spontaneously fill with water at relative humidity values above 95% (See Supporting Information Figure S7). In a practical sense, at relative humidity above 95%, water will condense inside the nanotubes and evaporate again when the relative humidity drops below 95%. The condensed water has a different refractive index to air; therefore the visual appearance of the nanotube coating should differ above and below 95% relative humidity. By exposing the nanotube coating to saturated water vapor, the change in visual appearance can be observed (see Supporting Information Movie S1, note the flat coating does not show the same change in optical properties). In contrast to nanorod structures, the presented nanotube coating can withstand the capillary force associated with evaporating water. The nanotube coating does not degrade in optical or wetting performance upon repeated exposure to the saturated water vapor. This is supporting evidence of the mechanical stability of the nanotubes compared to the nanorods.

CONCLUSION

In summary, we have demonstrated an easy way to produce large area nanotextured surfaces (ca squared centimeters) of a reflective material, the first reported to do so. The ordered nanotubes lead to a low reflectivity (light trapping) which opens its potential application such as in solar cell engineering. Furthermore, the nanotube structures are more mechanically stable than other nanostructures exampled by wetting experiments that can be done multiple times without destruction. In addition, the fast change of color due to differing humidity conditions promotes its application in a variety of sensor techniques.

ASSOCIATED CONTENT

Supporting Information

Figures S1−S7 and Movie S1. This material is available free of charge via the Internet at http://pubs.acs.org.

AUTHOR INFORMATION

Corresponding Author

*E-mail: drew.evans@unisa.edu.au. Fax: +61 8 83025639.

Notes

The authors declare no competing financial interest.

REFERENCES

(1) Chen, Q.; Hubbard, G.; Shields, P. A.; Liu, C.; Allsopp, D. W. E.; Wang, W. N.; Abbott, S. *Appl. Phys. Lett.* **2009**, *94*, 263118.
(2) Lin, Y. R.; Wang, H. P.; Lin, C. A.; He, H., Jr. *J. Appl. Phys.* **2009**, *106*, 114310.
(3) Qu, M.; Zhao, G.; Cao, X.; Zhang, J. *Langmuir* **2008**, *24*, 4185.
(4) Guo, P.; Zheng, Y.; Wen, M.; Song, C.; Lin, Y.; Jiang, L. *Adv. Mater.* **2012**, *24*, 2642.
(5) Liu, F.; Lee, J. Y.; Zhou, W. J. *Small* **2006**, *2*, 121.
(6) Jiang, C.; Markutsya, S.; Pikus, Y.; Tsukruk, V. V. *Nat. Mater.* **2004**, *3*, 721.
(7) Liu, N.; Tang, M. L.; Hentschel, M.; Giessen, H.; Alivisatos, A. P. *Nat. Mater.* **2011**, *10*, 631.
(8) Nositschka, W.; Beneking, C.; Voigt, O.; Kurz, H. *Sol. Energ. Mat. Sol. C.* **2003**, *76*, 155.
(9) Atwater, H. A.; Polman, A. *Nat. Mater.* **2010**, *9*, 205.
(10) Hobbs, K. L.; Larson, P. R.; Lian, G. D.; Keay, J. C.; Johnson, M. B. *Nano Lett.* **2004**, *4*, 167.
(11) Zheng, H.; Wang, J.; Lofland, S.; Ma, Z.; Mohaddes-Ardabili, L.; Zhao, T.; Salamanca-Riba, L.; Shinde, S.; Ogale, S.; Bai, F. *Science* **2004**, *303*, 661.
(12) Wu, H.; Zhang, R.; Liu, X.; Lin, D.; Pan, W. *Chem. Mater.* **2007**, *19*, 3506.
(13) Fu, J.; Cherevko, S.; Chung, C. H. *Electrochem. Commun.* **2008**, *10*, 514.
(14) Kumar, G.; Tang, H. X.; Schroers, J. *Nature* **2009**, *457*, 868.
(15) Sander, M. S.; Tan, L. S. *Adv. Func. Mater.* **2003**, *13*, 393.
(16) Losic, D.; Shapter, J. G.; Mitchell, J. G.; Voelcker, N. H. *Nanotechnology* **2005**, *16*, 2275.
(17) Evans, P.; Hendren, W.; Atkinson, R.; Wurtz, G.; Dickson, W.; Zayats, A.; Pollard, R. *Nanotechnology* **2006**, *17*, 5746.
(18) Fan, J. G.; Dyer, D.; Zhang, G.; Zhao, Y. P. *Nano Lett.* **2004**, *4*, 2133.
(19) Zuber, K.; Hall, C.; Murphy, P.; Evans, D. *Surf. Coat. Technol.* **2012**, *206*, 3645.
(20) Zuber, K.; Merkens, K.; Fröhlich, K.; Murphy, P.; Wong-Leung, J.; Evans, D. *Scr. Mater.* **2012**, *67*, 866.

Figure 6. Receding contact angle measurements on (A) flat, (B) nanotube, and (C) annealed coating. Texturing of the surface leads to hydrophilic behavior, whereas the flat coating of the same alloy material shows hydrophobic-like behavior.

(21) Evans, D.; Zuber, K.; Merkens, K.; Murphy, P. *Scr. Mater.* **2012**, *67*, 356.
(22) Hoffman, D. W.; Thornton, J. A. *Thin Solid Films* **1977**, *40*, 355.
(23) Thornton, J. A. *Annu. Rev. Mater. Sci.* **1977**, *7*, 239.
(24) Lyvers, D. P.; Moon, J. M.; Kildishev, A. V.; Shalaev, V. M.; Wei, A. *ACS Nano* **2008**, *2*, 2569.
(25) Yang, Z. P.; Ci, L.; James, A.; Lin, S. Y.; Ajayan, P. M. *Nano Lett.* **2008**, *8*, 446.
(26) Wenzel, R. N. *Ind. Eng. Chem.* **1936**, *28*, 988.
(27) Mason, G. *J. Colloid Interface Sci.* **1982**, *88*, 36.
(28) Thomson, W. *Philos. Mag.* **1871**, *42*, 448.